Design and Analysis of a Compact Penta-Band Polarization-Insensitive Bandstop Frequency Selective Surface

Anumoy Ghosh, Mukesh Kumar, *Student Member, IEEE*, Sk Nurul Islam, *Student Member, IEEE*, and Santanu Das, *Member, IEEE*

***Abstract*—A novel design of a compact penta-band frequency selective surface (FSS) is presented in this letter. The FSS unit cell consists of five metallic structures, two at the top surface and three at the bottom surface of the dielectric, which provide five stopbands in PCS, WiFi, CBRS, lower WLAN, and *X*-band downlink satellite communication frequency ranges. The mechanisms of stopband generations are elaborated with current distribution patterns and equivalent circuit modeling. The structure is polarization-insensitive and shows a stable response under oblique incidence up to $\pm 54^{\circ}$. The FSS unit cell is compact with dimensions $0.1\lambda \times 0.1\lambda$, where λ signifies the free-space wavelength corresponding to the lowest resonant frequency. A prototype of the proposed FSS is fabricated, and the measured results are in accord with the simulated results.**

***Index Terms*—Compact, frequency selective surface (FSS), oblique incidence angle, penta-band, polarization-insensitive.**

I. Introduction

A FREQUENCY selective surface (FSS) is ideally composed of an infinite array of periodically arranged metallic patches or slots that restrict or allow wave propagation at certain frequencies, thus behaving as bandstop or bandpass filter, respectively [1]. The bandstop property of the FSS is used in applications, such as electromagnetic shielding, antenna reflectors, and antenna beam shaping [2]–[4]. For the purpose of electromagnetic shielding, an FSS becomes more effective if it can act as a bandstop filter at as many wireless frequency bands as possible, while remaining transparent to other unused frequencies. Furthermore, because of space constraints in practical wireless applications, compact FSS unit cells are required such that numerous unit cells can be incorporated, which will closely resemble the filtering behavior of an ideal FSS [5]. Thus, the compact and multiband FSS acting as bandstop filters are desired. In addition, to conform with an extremely varying wireless communication path, the FSS structures should be polarization-insensitive and immune to the oblique incidence of electromagnetic waves.

In line with the aforementioned properties, various compact and multiband FSS have been presented in [6]–[13]. For the compact and multiband FSS design, various metallic loop structures are reported in [6]–[10]. However, achieving compactness and high stability under oblique incidence simultaneously remains a challenge. In fact, except for [12], no other triple-band FSS structure shows stable response under oblique incidence for more than $\pm 45^{\circ}$.

In this letter, the design of a penta-band FSS is proposed, which has five distinct stopband frequencies out of which three operating frequencies are closely spaced. The structure is compact, polarization-insensitive, and shows stability under oblique incidence up to $\pm 54^{\circ}$ angle of incidence. For the sake of experimental validation, the proposed FSS is fabricated and the measured results verify the simulated characteristics of the structure.

II. FSS Design Geometry

The proposed FSS unit cell is designed on an FR4 substrate with thickness 1.6 mm and loss tangent 0.02. Fig. 1(a) and (b) shows the configuration of metallic strips at the top and bottom surface of the FSS, respectively. The top surface is composed of a convoluted loop structure and a crossed dipole structure with meandered arms. The width of each microstrip section on the top surface is 0.3 mm. The bottom surface constitutes of three concentric loop structures. The largest loop is a conventional square ring with a strip width of 0.3 mm. The other two loops have meandered arms with a strip width of 0.5 mm. The relevant dimensions pertaining to the geometry of the unit cell are tabulated in Table I.

III. Results and Discussions

The $|S_{21}|$ plot of the proposed structure under normal incidence is presented in Fig. 2, which shows that the proposed structure provides transmission minima at five frequencies, thus acting as a penta-band bandstop filter. Furthermore, the figure also shows that the $|S_{21}|$ response is almost similar for both TE and TM modes of polarization. This property is because of the rotational symmetry (identical appearance of the structure when it is rotated through 90° around z-axis) of the FSS unit cell. The details of the resonant frequencies are listed in Table II, which also shows that five application bands are effectively shielded by the proposed structure while maintaining a compact size of 0.1λ

Manuscript received August 3, 2019; revised September 26, 2019; accepted November 6, 2019. Date of publication November 11, 2019; date of current version January 20, 2020. *(Corresponding author: Anumoy Ghosh.)*

A. Ghosh is with the Department of Electronics and Communication Engineering, National Institute of Technology Mizoram, Aizawl 796012, India (e-mail: anumoy.science@gmail.com).

M. Kumar, S. N. Islam, and S. Das are with the Department of Electronics and Telecommunication Engineering, Indian Institute of Engineering Science and Technology, Shibpur 711103, India (e-mail: mukeshnitd415@gmail.com; badshaays@gmail.com; santanumdas@gmail.com).

Digital Object Identifier 10.1109/LAWP.2019.2952689

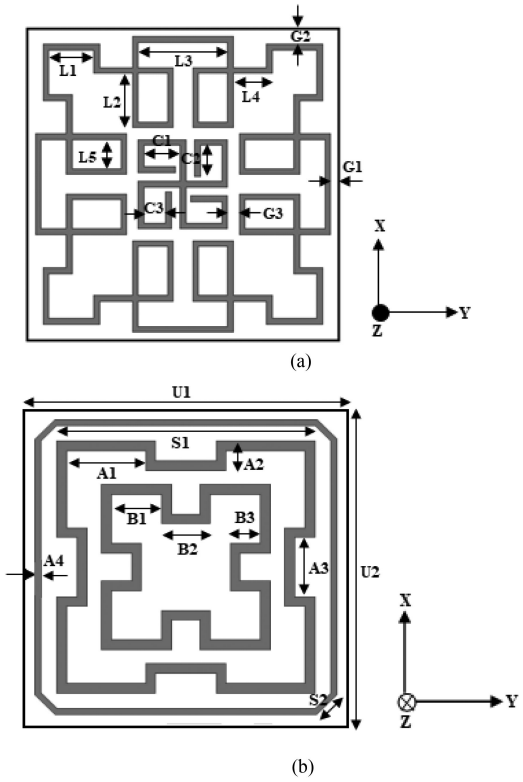

Fig. 1. Geometry of FSS unit cell: (a) top view and (b) bottom view.

TABLE I
DESIGN PARAMETERS OF THE FSS UNIT CELL (IN MILLIMETERS)

L1	L2	L3	L4	L5	C1	C2	C3	G1	G2	G3
2.3	2.8	4.6	2	1.5	1.85	1.6	1.1	0.4	0.8	0.6
S1	**S2**	**A1**	**A2**	**A3**	**A4**	**B1**	**B2**	**B3**	**U1**	**U2**
12.8	1.4	3.9	1.5	3	0.3	2.5	2.4	1.5	16	16

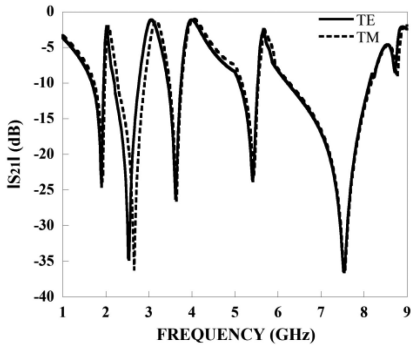

Fig. 2. Simulated $|S_{21}|$ response of the proposed FSS under normal incidence for both TE and TM polarizations.

$\times$ 0.1λ (λ is wavelength corresponding to the lowest resonant frequency). Fig. 1(b) shows modified corners of the outermost ring in order to decrease the overlap area between the outermost ring of the bottom layer and the convoluted ring of the top layer, thereby reducing the coupling between the first and second stopbands, which enhances the passband transmission between these two bands. It is observed from Fig. 2 that the transmission peaks are at –2.08 dB between the first and second stopbands, –1.04 dB between the second and third stopbands, –1.02 dB between the third and fourth stopbands, and –2.32 dB between the fourth and fifth stopbands, which are above –3 dB cut-off points, thus signifying satisfactory passband transmission outside the stopbands.

TABLE II
DETAILS OF OBTAINED STOPBAND RESONANCES

.	TE Mode		TM Mode		
Resonance no	Resonant Frequency (GHz)	Bandwidth (GHz)	Resonant Frequency (GHz)	Bandwidth (GHz)	Application band (GHz)
1	1.90	1.7 – 2.01	1.92	1.72 – 2.02	PCS (1.85-1.99)
2	2.46	2.2 – 2.76	2.51	2.23 – 2.84	WiFi (2.4-2.48)
3	3.62	3.45 – 3.75	3.63	3.46 – 3.77	CBRS (3.5-3.7)
4	5.42	5.14 – 5.56	5.44	5.16 – 5.55	Lower WLAN (5.15-5.35)
5	7.54	6.38 – 8.1	7.54	6.4 – 8.08	X-band downlink satellite communication (7.25-7.75)

The current distribution patterns of the proposed FSS at bandstop frequencies are investigated and presented in Fig. 3(a)–(e). The path marked by a1–a16 in Fig. 3(a) indicates the current path corresponding to the first resonance at 1.88 GHz. Similarly, the paths marked by b1–b4, c1–c5, d1–d5, and e1–e7 in Fig. 3(b)–(e) represent the flow of surface current at 2.5, 3.65, 5.44, and 7.58 GHz, respectively. Each path shows two current minima at the two ends of the path and a current maxima as the middle of the current path is approached, thus resembling a half-wavelength path corresponding to its resonance frequency. Furthermore, the meandered arms of the loops and the crossed dipole provide longer current paths as compared to conventional loop and crossed-dipole structures leading to lower resonance and achieving compactness.

The equivalent circuit of the FSS unit cell is shown in Fig. 4. Each of the metallic loops and the crossed dipole with meandered arms can be modeled as a series *LC* circuit [15], [16]. As each metallic structure has two half-wavelength current paths, the inductor is further simplified to be a parallel combination of two identical inductors. The bandstop resonant frequency because of each lumped LC circuit can be evaluated as follows: $f_i = 1/2\pi(0.5L_iC_i)^{1/2}$, i = 1,2,…,5, where *i* indicates the *i*th resonance. The dielectric substrate is modeled as a transmission line of characteristic impedance Z_D. The values of the lumped elements are derived as per the procedure mentioned in [6], and the calculated values are $L_1 = 90.64$ nH, $C_1 = 0.158$ pF, $L_2 = 27.53$ nH, $C_2 = 0.28$ pF, $L_3 = 22.19$ nH, $C_3 = 0.172$ pF, $L_4 = 16.05$ nH, $C_4 = 0.107$ pF, $L_5 = 12.32$ nH, and $C_5 = 0.27$ pF.

The performance of the proposed FSS under oblique incidence with different polarizations is shown in Fig. 5. From the figure, it is observed that the FSS maintains the stability till $\pm 54^\circ$ angle of incidence. A maximum frequency deviation of 0.33% and 0.12% is observed for the TE polarization at the second stopband and the TM polarization at the fifth stopband, respectively. The angular stability depends on the periodicity of the FSS structure, *D*, as follows [14]:

$$D < \frac{\lambda_o}{1 + \sin\theta}. \tag{1}$$

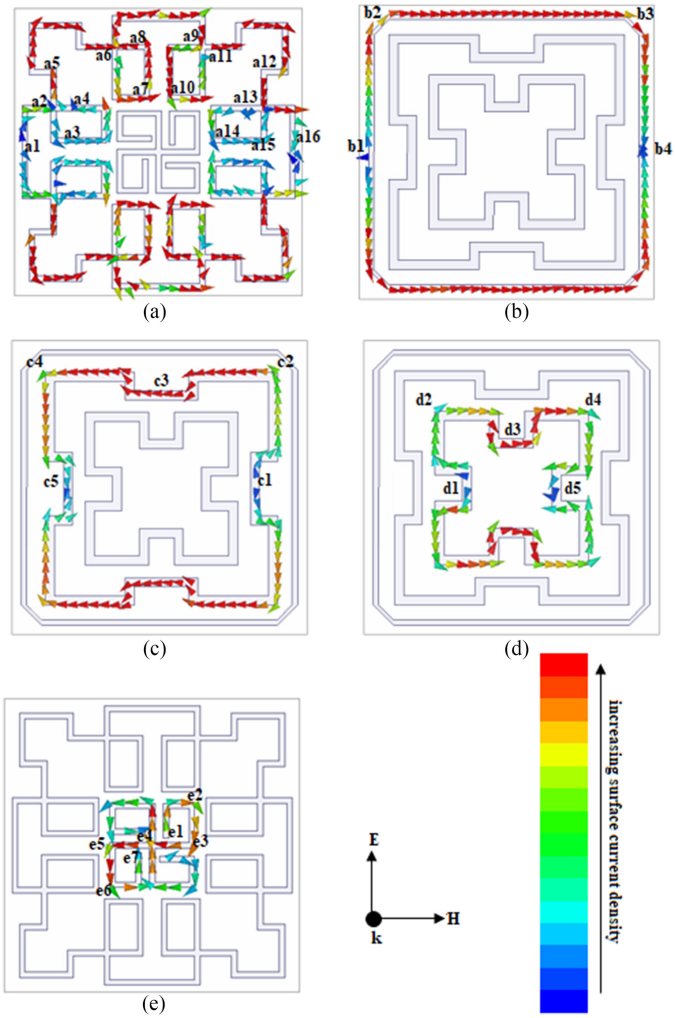

Fig. 3. Simulated surface current flow on the FSS surface at (a) 1.88, (b) 2.5, (c) 3.65, (d) 5.44, and (e) 7.58 GHz.

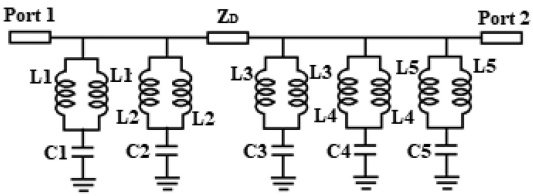

Fig. 4. Equivalent circuit for the proposed FSS unit cell.

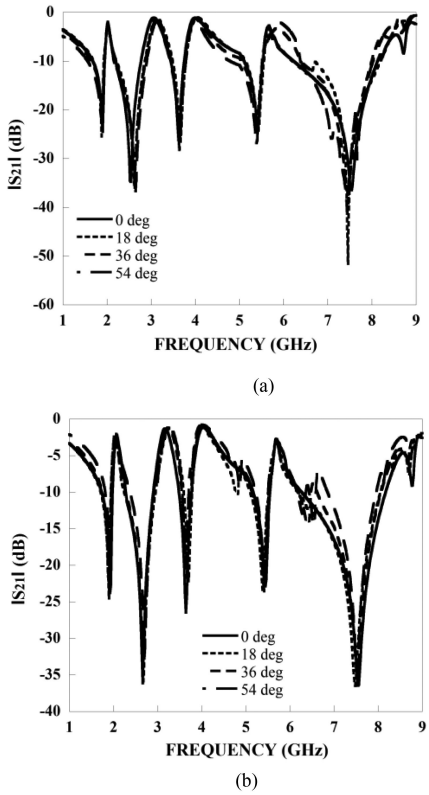

Fig. 5. Simulated $|S_{21}|$ characteristic of the proposed FSS under oblique incidence. (a) TE polarization. (b) TM polarization.

TABLE III
COMPARISON WITH SIMILAR FSS STRUCTURES

Ref.	No. of stopbands	Stability under oblique incidence	Unit cell size (in wavelengths corresponding to the lowest stopband resonance)	No. of metallic layers
[6]	2	75^0	0.065λ x 0.065λ	1
[7]	2	45^0	0.11λ x 0.11λ	1
[8]	2	45^0	0.42λ x 0.42λ	1
[9]	3	30^0	0.13λ x 0.13λ	1
[10]	2	60^0	0.16λ x 0.16λ	3
[11]	2	35^0	0.12λ x 0.12λ	2
[12]	3	45^0	0.16λ x 0.16λ	1
[13]	4	–	0.39λ x 0.39λ	1
Our Work	5	54^0	0.1λ x 0.1λ	2

Here, λ_0 is the free-space wavelength and θ is the angle of incidence. For angular stability, D should be reduced [14]. In the present case, at 54° incident angle, the limiting value of periodicity is $0.55\lambda_0$, whereas, for the lowest and highest frequencies, periodicity is $0.1\lambda_0$ and $0.4\lambda_0$, respectively, for the proposed structure, which is substantially lower than the limiting value, thus accounting for a good angular stability up to ±54° incidence angle. Fig. 5 shows that bandwidth increases slightly for TE and decreases for TM polarizations as incident angle increases because of wave impedance and hence quality factor enhancement for TE and reduction for TM modes [13].

Finally, in order to assess the advantage of the proposed design, a comparison between similar works involving the multi-band bandstop FSS is conducted, and the results are tabulated in Table III. The comparison reflects that the proposed structure shows five stopbands that are maximum thus being more advantageous than the dual or triple stopband FSS in terms of its utility in shielding electromagnetic radiation from numerous application bands. Furthermore, the triple bandstop FSS shows stability under oblique incidence till ±45°, which is improved in the proposed structure up to ±54°. The proposed structure is the most compact except for a dual-band FSS [6]. The comparison table shows that while most of the structures use a single metallic layer, they cannot provide more than three stopbands because the metallic layout becomes increasingly complex to be fabricated on a single layer without reducing the compactness as the number of stopbands increases. Thus, for five stopbands, either dual metallic layers or a bigger substrate area is required, but the latter

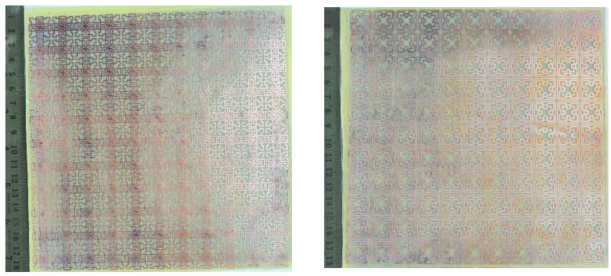

(a) (b)

Fig. 6. Photograph of the fabricated prototype. (a) Top view. (b) Bottom view.

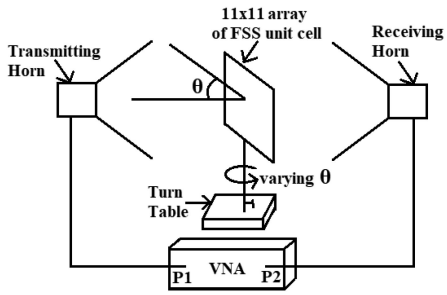

Fig. 7. Measurement set up for the FSS.

technique will compromise the compactness of the structure. Therefore, in the proposed structure, the top and bottom surfaces of a single substrate are used as two metallic layers, which neither affect the compactness nor the profile thickness. Hence, the comparison shows that the proposed FSS provides the most suitable tradeoff among multiband functionality, stability under oblique incidence, and compactness.

IV. Fabrication and Measurement

For experimental validation of the characteristics of the proposed FSS, a prototype is fabricated with 11×11 array of unit cells, and the photograph of the same is presented in Fig. 6. The $|S_{21}|$ response is measured using the free-space measurement technique as depicted in Fig. 7, which consists of appropriate horn antennas, the fabricated structure mounted on a turntable for measurement under oblique incidence, and a vector network analyzer (VNA) of make PNA-L 5235A. The prototype is placed in the far-field region of the horn antennas, a distance greater than $2D^2/\lambda$ from the antenna, where D is the largest dimension of the antenna and λ is the wavelength corresponding to the highest measured frequency. In the proposed work, multiple waveguide horn antennas of make NARDA-ATM are used (1.7–2.6, 2.6–3.95, 3.95–5.85, 5.85–8.20, and 8.2–12.4 GHz) to cover the measurement range of 1–9 GHz. The largest aperture area among these antennas and the FSS are 176×176 mm^2. Thus, the values of D (in this case, the diagonal length of the fabricated FSS [17]) and λ (corresponding to highest measured frequency) are 248.9 and 33.33 mm, respectively, and the far-field region is calculated to be beyond 3.7 m. During measurement, the distance between the antenna (both transmitting and receiving) and the prototype is kept at 3.8 m. The $|S_{21}|$ response without the prototype is measured and the data is used for calibration. The horn antennas are used in E- and H-planes for measurement under TE and TM modes of excitations, respectively. The horn antennas are chosen to have a wide half-power beamwidth of more than 35° at both

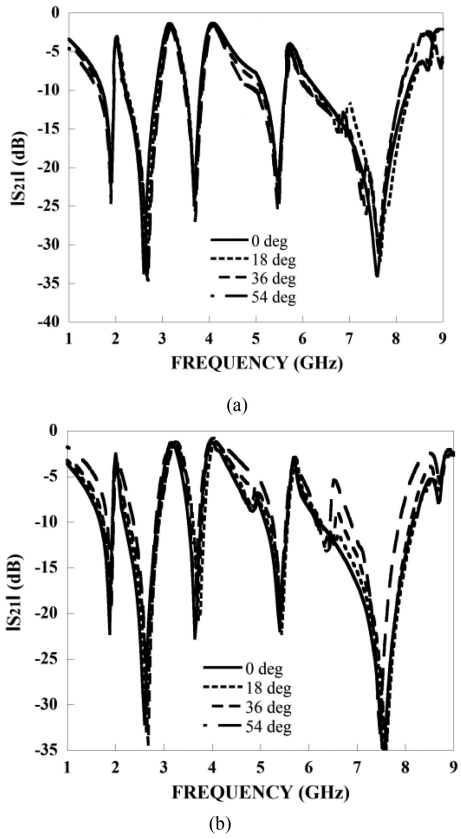

Fig. 8. Measured $|S_{21}|$ response under normal and oblique incidence. (a) TE polarization. (b) TM polarization.

the planes, and the horn apertures are considerably smaller than the surface area of the prototype (largest horn aperture is 96.28 cm^2, whereas the surface area of the prototype is 309.8 cm^2). These two factors enable satisfactory coupling of the transmitted electromagnetic waves to the FSS surface under a wide angle of incidence, which is essential for accurate measurement to validate the angular stability of the structure up to $\pm 54°$ [17]. The measured results are depicted in Fig. 8, which shows the close resemblance with the simulated transmission characteristics for both the polarizations under normal and oblique incidence. Although simulated results have shown almost unperturbed results under oblique incidence, there is some deviation in bandwidth at the stopbands along with some ripples during measurement under oblique incidence because of the limited number of FSS unit cells in the fabricated prototype and minor alignment errors.

V. Conclusion

In this letter, the design and analysis of a novel penta-band bandstop FSS have been proposed based on one crossed dipole and four closed-loop resonator structures with a compact cell size of $0.1\lambda \times 0.1\lambda$. The structure shows polarization insensitivity and has stable performance under oblique incidence. Its surface current density and equivalent circuit model have been presented to show the resonance mechanism. A comparison with the previously reported structures has established its superiority in the perspective of multiband functionality, immunity under oblique incidence, and compactness. A prototype of the proposed FSS has been fabricated, and the measured results confirm the simulated frequency characteristics with good accuracy.

REFERENCES

[1] B. A. Munk, *Frequency Selective Surface Theory and Design*. New York, NY, USA: Wiley, 2000.

[2] S. Ghosh and K. V. Srivastava, "Broadband polarization-insensitive tunable frequency selective surface for wideband shielding," *IEEE Trans. Electromagn. Compat.*, vol. 60, no. 1, pp. 166–172, Feb. 2018.

[3] J. Li, Q. Zeng, R. Liu, and T. A. Denidni, "A compact dual-band beam-sweeping antenna based on active frequency selective surfaces," *IEEE Trans. Antennas Propag.*, vol. 65, no. 4, pp. 1542–1549, Apr. 2017.

[4] G. Sen, T. Mandal, S. Majumdar, S. Mahato, S. Mondal, and P. P. Sarkar, "Design of a wide band frequency selective surface (FSS) for multiband operation of reflector antenna," in *Proc. 5th Int. Conf. Comput. Devices Commun.*, 2012, pp. 1–3.

[5] S. N. Azemi, K. Ghorbani, and W. S. T. Rowe, "Angularly stable frequency selective surface with miniaturized unit cell," *IEEE Microw. Wireless Compon. Lett.*, vol. 25, no. 7, pp. 454–456, Jul. 2015.

[6] S. Ghosh and K. V. Srivastava, "An angularly stable dual-band FSS with closely spaced resonances using miniaturized unit cell," *IEEE Microw. Wireless Compon. Lett.*, vol. 27, no. 3, pp. 218–220, Mar. 2017.

[7] S. Khajevandi, H. Oraizi, and M. Poordaraee, "Design of planar dual-bandstop FSS using square-loop-enclosing superformula curves," *IEEE Antennas Wireless Propag. Lett.*, vol. 17, no. 5, pp. 731–734, May 2018.

[8] S. Can, K. Y. Kapusuz, and A. E. Yilmaz, "A dual-band polarization independent FSS having a transparent substrate for ISM and Wi-Fi shielding," *Microw. Opt. Technol. Lett.*, vol. 59, no. 9, pp. 2249–2253, Sep. 2017.

[9] H. Nasrollahi, A. N. Yeganeh, S. H. Sedighy, and S. M. Ali-Nezhad, "Compact, dual polarized, mutliband frequency selective surface with wideband spurious rejection," *Microw. Opt. Technol. Lett.*, vol. 59, no. 4, pp. 888–893, Apr. 2017.

[10] F. Bagci, C. Mulazimoglu, S. Can, E. Karakaya, A. E. Yilmaz, and B. Akaoglu, "A glass based dual band frequency selective surface for protecting systems against WLAN signals," *AEÜ-Intl. J. Electron. Comm.*, vol. 82, pp. 426–434, Dec. 2017.

[11] J. Poojali, S. Ray, B. Pesala, K. C. Venkata, and K. Arunachalam, "Quad-band polarization-insensitive millimeter-wave frequency selective surface for remote sensing," *IEEE Antennas Wireless Propag. Lett.*, vol. 16, pp. 1796–1799, 2017.

[12] M. Kartal, J. J. Golezani, and B. Doken, "Triple band frequency selective surface design for GSM systems by utilizing a novel synthetic resonator," *IEEE Trans. Antennas Propag.*, vol. 65, no. 5, pp. 2724–2727, May 2017.

[13] B. Rahmati and H. R. Hassani, "Multiband metallic frequency selective surface with wide range of band ratio," *IEEE Trans. Antennas Propag.*, vol. 63, no. 8, pp. 3747–3753, Aug. 2015.

[14] A. Kocakaya and G. Cakir, "Novel angular-independent higher order band-stop frequency selective surface for X-band applications" *Microw., Antennas Propag.*, vol. 12, no. 1, pp. 15–22, Jan. 2018.

[15] D. Wang, W. Che, Y. Chang, K.-S. Chin, and Y. L. Chow, "A low-profile frequency selective surface with controllable triband characteristics," *IEEE Antennas Wireless Propag. Lett.*, vol. 12, pp. 468–471, 2013.

[16] N. Liu, X. Sheng, J. Fan, and D. Guo, "A miniaturized FSS based on tortuous structure design," *IEICE Electron. Exp.*, vol. 14, no. 2, pp. 1–7, Jan. 2017.

[17] H. F. Alvarez, M. E. de Cos Gomez and F. L. Heras, "Angular stability of metasurfaces: Challenges regarding reflectivity measurements," *IEEE Antennas Propag. Mag.*, vol. 58, no. 5, pp. 74–81, Oct. 2016.